

Article

Heteronuclear multidimensional NMR and homology modelling studies of the C-terminal nucleotide-binding domain of the human mitochondrial ABC transporter ABCB6

Kaori Kurashima-Ito^{a,b,c}, Teppei Ikeya^d, Hiroshi Senbongi^{a,†}, Hidehito Tochio^e,
Tsutomu Mikawa^{a,b,c}, Takehiko Shibata^{a,b,‡} & Yutaka Ito^{a,b,c,f,*}

^aCellular and Molecular Biology Laboratory, RIKEN, Wako, Saitama, 351-0198, Japan; ^bMolecular and Cellular Physiology Laboratory and ^cMolecular Biophysics Laboratory, International Graduate School of Arts and Sciences, Supramolecular Biology, Yokohama City University, Yokohama, Kanagawa, 230-0045, Japan; ^eCREST/Japan Science and Technology Agency (JST); ^dNational Institute of Advanced Industrial Science and Technology (AIST), Tokyo 135-0064, Japan; ^fDepartment of Chemistry, Tokyo Metropolitan University, Hachioji, Tokyo 192-0397, Japan

Received 16 December 2005; Accepted 10 March 2006

Key words: ABC transporter, mitochondria, NMR, nucleotide recognition

Abstract

Human ATP-binding cassette, sub-family B, member 6 (ABCB6) is a mitochondrial ABC transporter, and presumably contributes to iron homeostasis. Aimed at understanding the structural basis for the conformational changes accompanying the substrate-transportation cycle, we have studied the C-terminal nucleotide-binding domain of ABCB6 (ABCB6-C) in both the nucleotide-free and ADP-bound states by heteronuclear multidimensional NMR and homology modelling. A non-linear sampling scheme was utilised for indirectly acquired ¹³C and ¹⁵N dimensions of all 3D triple-resonance NMR experiments, in order to overcome the instability and the low solubility of ABCB6-C. The backbone resonances for approximately 25% of non-proline residues, which are mostly distributed around the functionally important loops and in the Helical domain, were not observed for nucleotide-free form of ABCB6-C. From the pH, temperature and magnetic field strength dependencies of the resonance intensities, we concluded that this incompleteness in the assignments is mainly due to the exchange between multiple conformations at an intermediate rate on the NMR timescale. These localised conformational dynamics remained in ADP-bound ABCB6-C except for the loops responsible for adenine base and α/β -phosphate binding. These results revealed that the localised dynamic cooperativity, which was recently proposed for a prokaryotic ABC MJ1267, also exists in a higher eukaryotic ABC, and is presumably shared by all members of the ABC family. Since the Helical domain is the putative interface to the transmembrane domain, this cooperativity may explain the coupled functions between domains in the substrate-transportation cycle.

Present addresses:

[†] Mitochondrial Diseases Group, MRC Dunn Human Nutrition Unit, Cambridge CB2 2XY, UK.

[‡] Shibata Distinguished Senior Scientist Laboratory, RIKEN, Wako, Saitama 351-0198, Japan.

*To whom correspondence should be addressed. E-mail: ito-yutaka@center.tmu.ac.jp

Introduction

Iron transportation across mitochondrial membranes is essential for the maintenance of mitochondrial functions, since many proteins involved in the oxidative phosphorylation process require a

Fe/S cluster in their catalytic centre (Beinert et al., 1997; Beinert and Kiley, 1999). On the other hand, the accumulation of excess amounts of Fe ions in mitochondria causes the synthesis of hydroxyl radicals by the Fenton reaction, which leads to the oxidative damage of mitochondrial DNA, lipids and proteins and consequently has an adverse effect on mitochondrial function (Stohs et al., 1995; Senbongi et al., 1999). Therefore, proteins involved in the homeostasis of Fe ions play a very important role in the normal functioning of mitochondria.

Human ATP-binding cassette, sub-family B, member 6 (ABCB6) was isolated as a homologue of *Saccharomyces cerevisiae* ATM1, which is the first ATP-binding cassette (ABC) transporter found in yeast (Leighton and Schatz, 1995). ABCB6 is a member of MDR/TAP subfamily of 49 human ABC transporters (Holland and Blight, 1999; Dean et al., 2001), and possesses only one trans-membrane domain (TMD) and a following nucleotide-binding domain (NBD) thereby classified as a “half” transporter. Molecular biological studies have suggested that ATM1 contributes to the export of Fe/S precursors from the mitochondrial matrix to the cytosol (Kispal et al., 1997, 1999). Similarly, ABCB6 localises in the mitochondrial inner membrane. The ATP-binding cassette, sub-family B, member 7 (ABCB7) is the other reported human homologue of ATM1, and shares 34% sequence identity with ABCB6 (Figure 1). The function of ABCB6 in human mitochondria has not been clarified. However, the overproduction of ABCB6 complemented ATM1 disruption in yeast, suggesting that ABCB6 exhibits a very similar biological function in human mitochondria (Mitsuhashi et al., 2000). ABCB7 is suggested to be responsible for some mitochondrial diseases, e.g. X-linked sideroblastic anaemia with ataxia (Allikmets et al., 1999). Exportation of Fe/S precursors is one of the proposed functions of ABCB7 (Csere et al., 1998). The biological functions of ATM1, ABCB6 and ABCB7, particularly the mechanism of ATP-induced conformational changes accompanying the substrate transportation cycle, must be considered on the common functional and structural bases of ABC transporters. It is highly probable that our ABCB6 shares a very similar mechanism of transportation, even though its substrate has not been identified.

The common substrate transportation cycle of ABC transporters has been proposed as follows (Higgins and Linton, 2004): In the basal state, the NBDs are in an open dimer configuration, with low affinity for ATP. Binding of the substrate to TMDs initiates the transport cycle, enhancing the ATP-binding affinity of the NBDs, and effectively lowering the activation energy for closed dimer formation. Then the closed dimer induces a conformational rearrangement of the TMDs and simultaneously reduces the affinity for the substrate, promoting its release. Finally ATP is hydrolysed, and the sequential release of inorganic phosphate and ADP restores the transporter to its basal configuration. According to this cycle, conformational coupling between the NBDs and the TMDs is indispensable for the normal functioning of transporters. The recognition of bound nucleotide (ADP, ATP or none) on the NBDs must be communicated to the TMDs correctly, while the existence of substrate on the TMD must be transmitted to the residues responsible for controlling affinity to ATP. While there are partial explanations of this common regulation mechanism, no explanation has fully addressed the experimentally observed details.

High-resolution X-ray structures of NBDs from ABC transporters have shown a very similar tertiary fold composed of the RecA-like domain (or the ATPase core domain) and the Helical domain (or ABC α subdomain), in which the conserved amino acid motifs contribute to the nucleotide-binding pocket (Higgins and Linton, 2004). The Walker A motif (or P-loop) and the Walker B motif, which are common to nucleotide binding and hydrolysing proteins, form hydrogen bonds extensively with the bound nucleotide. It has been proposed that the function of the Walker B motif, which forms a β -strand, is to help coordinate the Mg^{2+} ion, possibly through a water molecule (Hopfner et al., 2000; Smith et al., 2002), or to polarise the attacking water molecule (Hung et al., 1998). In addition, ABC NBDs, including those without transport functions, e.g. MutS and Rad50, share three other peculiar motifs: (1) the well-conserved signature motif (consensus LSGGQ), which is proposed to be a γ -phosphate sensor in the opposing molecule of the dimer (Hopfner et al., 2000; Smith et al., 2002), (2) the Q-loop (also referred to as the “lid”) that contains a glutamine residue interacting with the γ -phos-

ABCB6-C	558	FIDMENMFDLLKEETEVEKDLPGAGPLRF--QKGR-IEFENVHFSY--ADGRETLQDVSFVMPGQTLALVGP	SGA
ABCB7	438	LIDMNTLFTLLKVDTPQIKDKVMASPLQITPQTAT-VAFDNVHFEY--IEGQKVLSGISFEVPAGKKVAIVGSSGS	
Atm1p	427	LIDMETLFLKLRKNEVKIKN--AERPLMLPENVPYDITFENVTFGY--HPDRKILKNASFTIPAGWKTAVGSSGS	
TAP1c	489	-----GLL-----TPLHL---EGL-VQFQDVSFAYpnrPDVVLVQLGTLFTLRPGEVTALVGPNGS	
LmrA	1	-----M-LSARHVDFAY--DDSEQILRDISFEAQPNSTIAFAGPSGG	WalkerA
ABCB6-C	628	GKSTILRLLFRFYDISSGCIRIDQDISQVTQASLRSHIGVVPQDTVLFNDTIADNIRYGRV-TAGNDEVEAAAQ	
ABCB7	510	GKSTIVRLLFRFYEPQKGSIIYLAGQNIQDVSLESRRRAVGVVQDAVLFHNTIYYNLLYGNI-SASPEEVYAVAK	
Atm1p	560	GKSTILKLVFRFYDPESGRILINGRDIKEYDIDALRKVIGVVPQDTPLFNDTIWENVKFGRI-DATDEEVIITVVE	
TAP1c	540	GKSTVAALLQNLQPTGGQLLDGKPLPQYEHRYLHRQVAAVGQEPQVFGRSLOENIAYGLTKPTMEEITAAV	
LmrA	40	GKSTIFSLLEFRFYQPTAGEITIDGQPIDNISLENWRSQIGFVSDSAIMAGTIRENLTYGLEGDYTDDELWQVLD	WalkerA
			Q-loop
ABCB6-C	702	AAGIHDAIMAFPEGYRTQVGERGLKLSGGEKQRVAIARTILKAPGIILLDEATSALDTSNERAIQASLAKVCA--	
ABCB7	584	LAGLHDAILRMPHGYDTQVGERGLKLSGGEKQRVAIARAILKDPVILYDEATSSLDTSITEETILGAMKDVVK--	
Atm1p	634	KAQLAPLIKLPQGFDTIVGERGLMISGGEKQRLAIARVLLKNARIMFFDEATSALDTHTEQALLRTIRDNFTSG	
TAP1c	615	KSGAHSFISGLPQGYDTEVDEAGSQLSGGQRQAVALARALIRKPCVLIILDDATSALDANSOLQVEQLLYESPERY	
LmrA	115	LAFARSFVENMPDQLNTEVGERGVKISGGQRQLAIARAFLRNPKILMLDEATASLDSESE-SMVQKALDSLM-K	
		Signature motif	WalkerB D-loop
ABCB6-C	775	NRTTIVVAHRLSTVNVADQILVIKDCGIVERGRHEALLSRGGVY-ADMWQLQQGQEETSEDTKPQTMR	
ABCB7	657	HRTSIFIAHRLSTVVDADKIIIVLDQKVAERGTHHGLLANPHSIYSEMWHQSSRVQNHNDNPKWEAKKE	
Atm1p	709	SRTSVYIAHRLRTIADADKIIIVLDNGRVREEGKHLELLAMPGLYRELWTIQEDLDHLENELKDQQL-	
TAP1c	690	SRSVLLITQHLSTLVEQADHILFLEGGAIREGGTHQQLMEKGCY----WAMVQAPADAPE-----	
LmrA	188	GRTTLVIAHRLSTIVDADKIYFIEKGQITGSGKHNELVATHPLY-AKYVSEQLTVQG-----	
			H-motif

Figure 1. Sequence alignment of the C-terminal region (residues 558–842) of human ABCB6 with the corresponding regions of other mitochondrial ABC half transporters, human ABCB7 (Allikmets et al., 1999; Csere et al., 1998) and *Saccharomyces cerevisiae* Atm1p (Leighton and Schatz, 1995). The sequences of human TAP1 (Kelly et al., 1992) and *Lactococcus lactis* LmrA (van Veen et al., 1998), whose structures were used for homology modelling of ABCB6-C, were also aligned. Identical residues are coloured yellow. Conserved sequence motifs are shown with bars.

phate through a water, which is the plausible attacking nucleophile (Hopfner et al., 2000; Smith et al., 2002; Hung et al., 1998), and (3) the switch region (also referred to as the H-motif) (Schneider and Hunke, 1998) that contains a conserved histidine, which has also been postulated to polarize the attacking water molecule for hydrolysis (Hopfner et al., 2000; Smith et al., 2002).

For the detection of the dynamic rearrangement of the structure of NBDs in response to ADP/ATP-binding, solution NMR approaches are useful tools. For other nucleotide-binding proteins, e.g. human Ras GTPase, changes in local conformational flexibility in response of the GDP/GTP-binding have indeed been found to be responsible for the binding events with downstream effectors (Geyer et al., 1996; Ito et al., 1997). Any structural knowledge obtained in aqueous solution is therefore required to complement the existing X-ray data. However, because of the NMR methodological requirements, such as

size-limitation, solubility and so on, the NBDs, but not as the whole transporters including the TMDs, are the most sensible targets for the detailed analyses.

Recently, heteronuclear multidimensional NMR has been applied to MJ1267, the first example of its use on an ABC transporter. MJ1267 is a separate ABC subunit of the branched-chain amino acid transporter system in the hyperthermophilic archaeon *Methanococcus jannaschii* (Wang et al., 2002, 2004). Using backbone ^{15}N relaxation analysis, the flexibilities on the μs -ms time scale in several key ABC motifs were found, these were in the loop region following the Walker B motif, the Q-loop, the H-motif, the signature motif and the LivG insert (a unique sequence element shared among branched-chain amino acid transporters) in the Helical domain. In combination with chemical shift perturbation analysis, it was concluded that the “selected-fit” model (James and Tawfik, 2003) for nucleotide binding contrib-

utes the allosteric changes in conformational dynamics in the LivG insert. Applying NMR to ABC transporters from higher organisms will result in an understanding of the common mechanism shared by all ABC proteins.

In the present study, we applied the uniform $^2\text{H}/^{13}\text{C}/^{15}\text{N}$ -labelling and triple-resonance NMR technique (Ikura et al., 1990) to the 31.5-kDa C-terminal fragment of ABCB6 (ABCB6-C) comprising residues from Phe558 to the C-terminal Arg842, in which residues corresponding to the NBD are included. To the best of our knowledge, this is the first triple-resonance NMR study on the NBDs of eukaryotic ABC transporters. We describe the backbone resonance assignments and secondary structures of ABCB6-C in the nucleotide free- and the ADP-bound states. We also performed homology modelling of ABCB6-C, which was used to interpret the obtained NMR data including the chemical shift perturbation upon the ADP-binding.

Materials and methods

Expression and purification of ABCB6-C

DNA encoding the ABCB6 gene corresponding to Phe558–Arg842 (ABCB6c) was a kind gift from Dr N. Mitsuhashi (Chiba University). For the expression of ABCB6-C, the ABCB6c DNA was subcloned into the *EcoRI* and *XhoI* sites in pGEX-4T (Amersham Biosciences), and the resultant expression plasmid was introduced into *Escherichia coli* strain BL21-CodonPlus®-RIL (Stratagene).

For NMR experiments, uniformly ^2H , ^{13}C and ^{15}N -labelled ($^2\text{H}/^{13}\text{C}/^{15}\text{N}$ -) ABCB6-C protein was prepared as a GST-fusion protein by growing the transformed bacteria in 90% $^2\text{H}_2\text{O}$ M9 minimal medium containing 1 g/l $^{15}\text{NH}_4\text{Cl}$ and 4 g/l [$^{13}\text{C}_6$] D-glucose, as the sole nitrogen and carbon sources, respectively. For the preparation of uniformly ^2H and ^{15}N -labelled ($^2\text{H}/^{15}\text{N}$ -) ABCB6-C protein, ^{13}C -labelled D-glucose was replaced by the same concentration of unlabelled D-glucose. At $\text{OD}_{600\text{nm}}$ of ~ 0.4 , the incubating temperature was shifted from 37 °C to 18 °C and protein expression was induced by the addition of isopropyl thio- β -D-thiogalactoside (IPTG) to a final concentration of 1 mM. After 30 h of further

growth at 18 °C, the cells were harvested, washed, and stored at -80 °C. In addition to the stable isotope-enriched proteins, unlabelled ABCB6-C was also obtained for biochemical experiments by expressing in LB media.

All the purification procedures described below were carried out at 4 °C. The cell pellet was suspended in lysis buffer [10 mM sodium phosphate, 1.8 mM potassium phosphate (pH 7.3), 140 mM NaCl, 0.7 mM KCl, 5 mM DTT, and 1% Triton X-100 (Sigma)]. Lysis was performed by two passages of sonication after adding lysozyme (0.1 mg/ml). The cell debris was clarified by centrifugation at 60,000g for 1 h. The GST-tagged ABCB6-C was purified using a glutathione agarose affinity column (Sigma). The cleavage of the GST-tag was achieved by biotinylated thrombin (Novagen) on the column, and ABCB6-C was eluted while the cleaved GST-tag was remaining bound to the column. ABCB6-C containing solutions was then loaded onto Resource Q (Amersham Biosciences) anion exchange column pre-equilibrated with purification buffer [50 mM Tris-HCl (pH 7.5) and 5 mM DTT] and eluted using a NaCl gradient. The final ABCB6-C fractions were collected and concentrated.

NMR spectroscopy

All NMR experiments presented in this report were performed in a triple-resonance CRYO-PROBE fitted with a Z-axis pulsed field gradient coil, using a 600 MHz Bruker DRX spectrometer at the Advanced Development and Supporting Center, RIKEN, with the exception of 2D ^1H - ^{15}N TROSY-HSQC (Pervushin et al., 1997) spectra measured on a 800 MHz Bruker DRX spectrometer at Tokyo Metropolitan University. All NMR spectra were processed on LINUX-PCs using the Azara 2.7 suite of software (Boucher, <http://www.bio.cam.ac.uk/azara/>), and visualised and analysed on LINUX-PCs with the combination of customised macro programs on the OpenGL-version of ANSIG 3.3 software (Kraulis, 1989; Kraulis et al., 1994).

NMR titration experiments of ABCB6-C with ADP

A series of 2D ^1H - ^{15}N TROSY-HSQC spectra were measured on $^2\text{H}/^{15}\text{N}$ -labelled ABCB6-C with unlabelled ADP at various protein:nucleo-

tide ratios in order to monitor gradual changes in the chemical shifts or intensity of ^1H - ^{15}N correlation cross-peaks of ABCB6-C. Two different conditions, (1) at pH 7.5 and 5 °C probe temperature and (2) at pH 8.5 and 25 °C probe temperature, were employed. Purified $^2\text{H}/^{15}\text{N}$ -labelled ABCB6-C was dissolved in either NMR buffer A [90% $^1\text{H}_2\text{O}/10\%$ $^2\text{H}_2\text{O}$ containing 20 mM $\text{Na}_2\text{HPO}_4\text{-NaH}_2\text{PO}_4$ (pH 8.5), 5 mM MgCl_2 , 50 mM Na_2SO_4 , 5 mM DTT, and 10 μM APMSF] or NMR buffer B (identical to NMR buffer A except that the pH was 7.5) and concentrated (~ 0.1 mM).

2D ^1H - ^{15}N TROSY-HSQC spectra were acquired with 16 transients and a total of 1024 (t_2 , $^1\text{H}^{\text{N}}$) \times 128 (t_1 , ^{15}N) complex points. Initially, a reference spectrum was recorded in the absence of ADP. Then the sample was taken out of the NMR tube and mixed with a 100 mM ADP solution to achieve a protein:nucleotide molar ratio of 1:0.5, prior to the next measurement. More nucleotide solution was added incrementally to measure ^1H - ^{15}N TROSY-HSQC spectra at protein:nucleotide molar ratios of 1:1, 1:2, 1:4, 1:8, 1:16 and 1:32. Note that the concentration of Mg^{2+} in the solution was always larger than that of ADP during this titration experiments. The concentration of the protein was not adjusted after each titration point due to the small volume of the ADP solution that was added.

NMR methods for backbone resonance assignments

Backbone $^1\text{H}^{\text{N}}$, ^{15}N , $^{13}\text{C}^{\alpha}$, $^{13}\text{C}'$, and side-chain $^{13}\text{C}^{\beta}$ resonance assignments were performed on $^2\text{H}/^{13}\text{C}/^{15}\text{N}$ -labelled ABCB6-C (~ 0.2 mM) under four different conditions, (1) in the absence of ADP, at pH 7.5 and 5 °C probe temperature, (2) in the absence of ADP, at pH 8.5 and 25 °C probe temperature, (3) in the presence of ADP, at pH 7.5 and 5 °C probe temperature, and (4) in the presence of ADP, at pH 8.5 and 25 °C probe temperature. For the measurements in the presence of ADP, unlabelled ADP was added to a final concentration of 3.2 mM (protein:ADP = 1:16), prior to the measurements. Six 3D triple-resonance NMR spectra, HNCA (Grzesiek and Bax, 1992; Yamazaki et al., 1994a), HN(CO)CA (Bax and Ikura, 1991; Yamazaki et al., 1994b), HN(CA)CB (Wittekind and Mueller, 1993; Yamazaki et al., 1994b), HN(COCA)CB (Yamazaki et al., 1994b),

HNCO (Grzesiek and Bax, 1992), and HN(CA)-CO (Clubb et al., 1992; Matsuo et al., 1996) with deuterium-decoupling and TROSY-modification (Salzmann et al., 1999a, b) were measured.

To reduce experimental time, a non-linear sampling method (Barna et al., 1987; Schmieder et al., 1994; Rovnyak et al., 2004) was utilised for the indirectly observed ^{15}N and ^{13}C dimensions. Briefly, 16 (^{15}N) and 14 (^{13}C) non-linear complex points were selected out of 24 (^{15}N) and 24 (^{13}C) conventional linear sampling points. For the acquisition dimension ($^1\text{H}^{\text{N}}$) of 3D experiments, 512 complex points were measured. The two-dimensional maximum entropy method (Laue et al., 1996) was used for processing of non-linearly sampled ^{13}C and ^{15}N dimensions with improved resolution. The efficiency of this combination of non-linear sampling and 2D maximum entropy processing has been carefully examined by using several 3D triple-resonance NMR data obtained on samples with similar molecular size as ABCB6-C.

Buffer pH, probe temperature and magnetic field strength dependencies of the ^1H - ^{15}N TROSY-HSQC Spectra

A series of ^1H - ^{15}N TROSY-HSQC spectra were measured on $^2\text{H}/^{13}\text{C}/^{15}\text{N}$ -labelled ABCB6-C (~ 0.1 mM) under the following variable conditions, (a) with/without ADP, (b) buffer pH of 7.5, 8.0, and 8.5, and (c) probe temperatures of 5, 15, and 25 °C. NMR buffer C (identical to NMR buffers A and B except that the buffer pH was adjusted to 8.0) was used for the preparation of ABCB6-C samples at pH 8.0. At pH 7.5, probe temperature 5 °C, additional ^1H - ^{15}N TROSY-HSQC spectra were measured for both ABCB6-C on its own and in the presence of ADP at a field of 18.8 T (the ^1H frequency of 800 MHz). These 2D TROSY-HSQC spectra were acquired with 1024 (t_2 , $^1\text{H}^{\text{N}}$) \times 128 (t_1 , ^{15}N) complex points. Resolution enhancement for ^{15}N -dimension was achieved by applying linear prediction (Zhu and Bax, 1990) prior to Fourier transformation.

Homology modelling

In order to interpret the obtained NMR data, we performed homology modelling of ABCB6-C.

First, a homology search was performed using the FORTE program (Tomii and Akiyama, 2004). Template structures for homology modelling were selected by analysing structures from FORTE with high *Z*-scores using PSI-BLAST (Altschul et al., 1997) and the VAST Search service of National Center for Biotechnology Information, U.S.A. (<http://www.ncbi.nlm.nih.gov/Structure/VAST/vast.shtml>) (Madej et al., 1995). The structure with the highest *Z*-score from FORTE was nucleotide-binding domain 1 of the cystic fibrosis transmembrane conductance regulator (PDB ID: 1Q3H) (Lewis et al., 2004). However, this structure was not used as the template for modelling because of relatively low sequence identity (~27%). The structures with the second and third highest *Z*-scores were the NBD of human TAP1 (PDB ID: 1JJ7) (Gaudet and Wiley, 2001) and the NBD of *Lactococcus lactis* LmrA (PDB ID: 1MV5), respectively. Since these two structures were categorised into one structure similarity group, we selected the structure of LmrA NBD, which has higher sequence identity, as the template. On the other hand, two other structures, *E. coli* MsbA (PDB ID: 1JSQ) (Chang and Roth, 2001) and *Vibrio cholera* MsbA (PDB ID: 1PF4) (Chang, 2003), which belong to the other structure similarity group, were found using PSI-BLAST and VAST, and they had relatively high sequence identities with ABCB6. The NBD part of the *Vibrio cholera* MsbA structure was selected as the representative structure, because the *E. coli* structure includes only CA coordinates.

We performed homology modelling with both pair wise (using the structure of LmrA NBD) and multiple alignments (using the structures of LmrA and *Vibrio cholera* MsbA NBDs) to obtain the most dependable prediction structures possible. As the first step, homology modelled structures were calculated using the program MODELLER version 7.7 (Šali and Blundell, 1993) with dihedral angle constraints for backbone ϕ and ψ angles generated from the calculation of Chemical Shift Index (CSI) method (Wishart and Sykes, 1994) using $^{13}\text{C}^\alpha$, $^{13}\text{C}^\beta$ and $^{13}\text{C}'$ chemical shifts. Since two sets of acceptable structures calculated using either pair wise or multiple alignment exhibited good agreement each other (the root mean square deviation of backbone heavy atoms for residues 33–270 was about 2.9 Å), we concluded that these structures were reliable, and therefore used the

structures with pair wise alignment in the following step. Second side-chain modelling was performed using SCWRL version 3.0 (Canutescu et al., 2003). For each modelling step, 15 acceptable structures were extracted from 50 calculated structures. The structure with the lowest values of objective function was selected as the representative structure, and used for discussions. All PSI-BLAST, MODELLER and SCWRL calculations were performed on a LINUX-PC cluster system.

Results

Interaction of ABCB6-C with ADP

Fluorescence studies have shown ADP/ATP binding by the NBD of ATM1 (ATM1-C) with dissociation constants of ~43 and ~97 μM (pH 7.3), respectively (Chen and Cowan, 2003). We tried to apply a similar approach to the interaction of ABCB6-C with ADP, and found the dissociation constant to be ~50 μM (data not shown). The interaction of ABCB6-C with ATP was difficult to characterise because of its intrinsic ATPase activity (data not shown). The interactions of ABCB6-C with ADP was also characterised by CD spectroscopy (data not shown).

Preparation of ABCB6-C samples for NMR measurements

Triple resonance NMR experiments usually require high sample concentration (~1 mM). For the analysis of relatively larger proteins, like ABCB6-C, four to six 3D triple-resonance NMR spectra are usually measured in order to reduce the ambiguity caused by signal overlapping, and each requires 1–3 days measurement time. The less concentrated the sample, the more measurement time is needed to achieve reasonable sensitivity.

Publications have so far described the NBDs of ABC transporters as difficult to be concentrated and when it is concentrated, it tends to aggregate after a relatively short period (Yuan et al., 2001; Chen and Cowan, 2003). The hydrophobic nucleotide-binding pocket of this domain has been suggested to be responsible for non-specific hydrophobic interactions at higher concentration, thus causing the low solubility of ABC domains.

Despite being highly purified, ABCB6-C samples were found to be unstable at room temperature (25 °C) and easily precipitated, presumably by non-specific aggregation. ABCB6-C was found to be most stable under mildly alkaline conditions, and shifting the buffer pH to neutral or mildly acidic conditions resulted in quicker precipitation. Further optimisations of buffer conditions, e.g. addition of L-arginine and L-glutamate simultaneously (Golovanov et al., 2004), showed no apparent effect on improving protein solubility and long-term stability. The lifetime of ABCB6-C at pH 8.5 and 25 °C was estimated by monitoring the intensities of ^1H - ^{15}N correlation cross peaks in 2D ^1H - ^{15}N HSQC spectra measured on ^{15}N -labelled ABCB6-C. At the sample concentration range under 0.1 mM, the signal intensity was approximately halved after 12 h (data not shown). No significant concentration dependence was found in 2D ^1H - ^{15}N HSQC spectra upon increasing the concentration from below 0.1–0.4 mM. Higher concentrations (>0.5 mM) provided a quicker drop of intensity during the measurements.

NMR studies of proteins over 200 amino acids in length have been made easier with the advent of

deuteration. Complete deuteration of all but the exchangeable $^1\text{H}^{\text{N}}$ protons in such large proteins improves the sensitivity of triple-resonance NMR experiments (Grzesiek et al., 1993; Yamazaki et al., 1994a). Thus, 80%–85 % deuterated ABCB6-C samples were prepared and used for the NMR titration experiments and backbone resonance assignment.

Titration experiments of ABCB6-C with ADP

Preliminary NMR experiments were carried out to confirm the adenine nucleotide-binding activities of ABCB6-C by measuring 2D ^1H - ^{15}N HSQC spectra of ^{15}N -labelled ABCB6-C with excess amounts of ADP. By comparison with 2D ^1H - ^{15}N HSQC spectrum of ABCB6-C on its own, addition of ADP caused many changes in chemical shift as well as the appearance of new cross peaks.

Next, we performed a series of stepwise, multipoint NMR titration experiments with ADP as presented in Figure 2. Considering its short lifetime at room temperature, uniform ^2H -labelling and application of a TROSY experimental scheme (Pervushin et al., 1997) were used to achieve improved resolution and sensitivity. 2D ^1H - ^{15}N

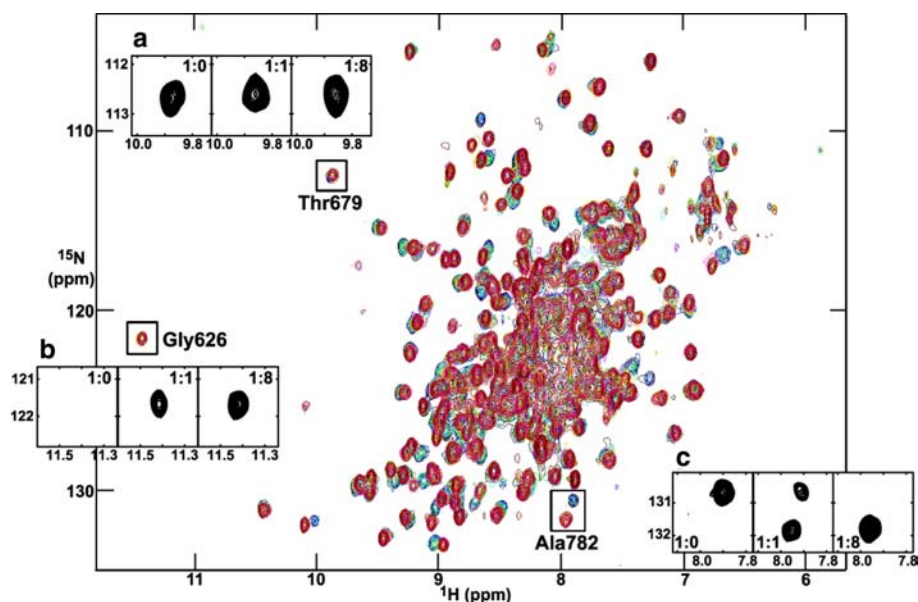


Figure 2. Overlays of 2D ^1H - ^{15}N TROSY-HSQC spectra from multipoint titrations of $^2\text{H}/^{15}\text{N}$ -labelled ABCB6-C with unlabelled ADP. The colour codes of ^1H - ^{15}N correlation cross peaks at each point, showing the molar ratio of ABCB6-C:ADP, are as follows: black (1:0); blue (1:0.5); cyan (1:1); green (1:2); yellow (1:4); orange (1:8); magenta (1:16); red (1:32). Shown as insets are representative cross-peaks for the slow exchange between free and ADP-bound ABCB6-C: (a) no change in shift or intensity (Thr679); (b) emerging (Gly626); (c) co-existence of the nucleotide-free and ADP-bound states (Ala782).

TROSY-HSQC spectra were measured, first in the absence of ADP and then at each titration point, to monitor the ^1H - ^{15}N correlation cross-peaks during ligand-binding.

ADP addition affected large numbers of ABCB6-C resonances in one of the following three ways: (1) no change in intensity and chemical shift or minor perturbation in chemical shift (Figure 2a), (2) disappearing cross-peaks, and (3) emerging cross-peaks (Figure 2b). These changes were initially observed upon the first point of titration (protein:nucleotide molar ratio of 1:0.5), and were almost saturated at around a protein:nucleotide molar ratio of 1:8–1:16.

A slow exchange regime on the NMR time-scale may exist between the nucleotide free- and ADP-bound states, since disappearing and emerging cross-peaks were observed simultaneously. In fact, a few pairs of cross-peaks were indeed identified as the possible distinct sets, corresponding to the co-existence of the nucleotide-free and ADP-bound states during the titration (Figure 2c).

Backbone assignment and secondary structure of ABCB6-C in the nucleotide-free state

The assignments of backbone $^1\text{H}^{\text{N}}$, $^{13}\text{C}^{\alpha}$, $^{13}\text{C}'$, ^{15}N and side-chain $^{13}\text{C}^{\beta}$ resonances of ABCB6-C in the nucleotide-free state were first performed at pH 8.5 and a probe temperature of 25 °C. We applied a non-linear sampling scheme (Barna et al., 1987; Schmieder et al., 1994; Rovnyak et al., 2004) for the indirect dimensions of all of these 3D experiments, which enabled us to measure spectra of equivalent quality with approximately 1/3 duration, when compared with employing a conventional sampling scheme. By analysing the spin-spin connectivities in the six 3D spectra, 202 of 276 (73%) non-proline residues in ABCB6-C (ABCB6-C has eight proline residues) were assigned. The $^1\text{H}^{\text{N}}$, $^{13}\text{C}^{\alpha}$, $^{13}\text{C}^{\beta}$, $^{13}\text{C}'$, and ^{15}N chemical shifts have been deposited in the BioMagResBank (<http://www.bmrb.wisc.edu>) database under the accession number BMRB-10016. In the ^1H - ^{15}N TROSY-HSQC spectrum (provided as supplementary material with the assignments indicated for the individual cross peaks), less than 30 separately observed cross peaks remained unassigned. Among them, ten $^1\text{H}^{\text{N}}$ - ^{15}N correlation cross peaks showed

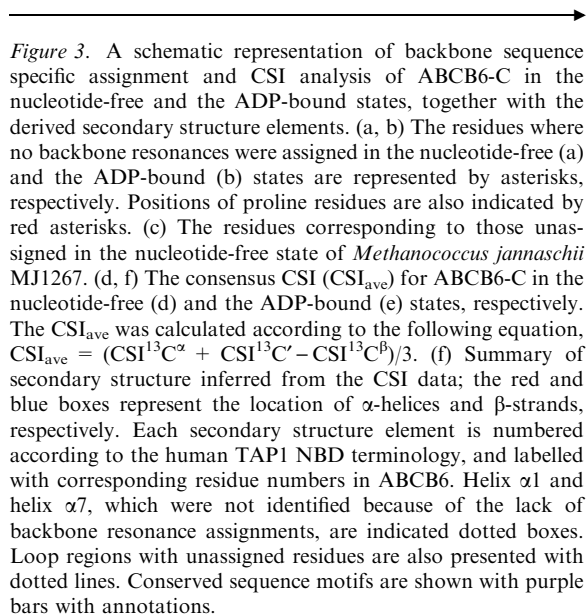
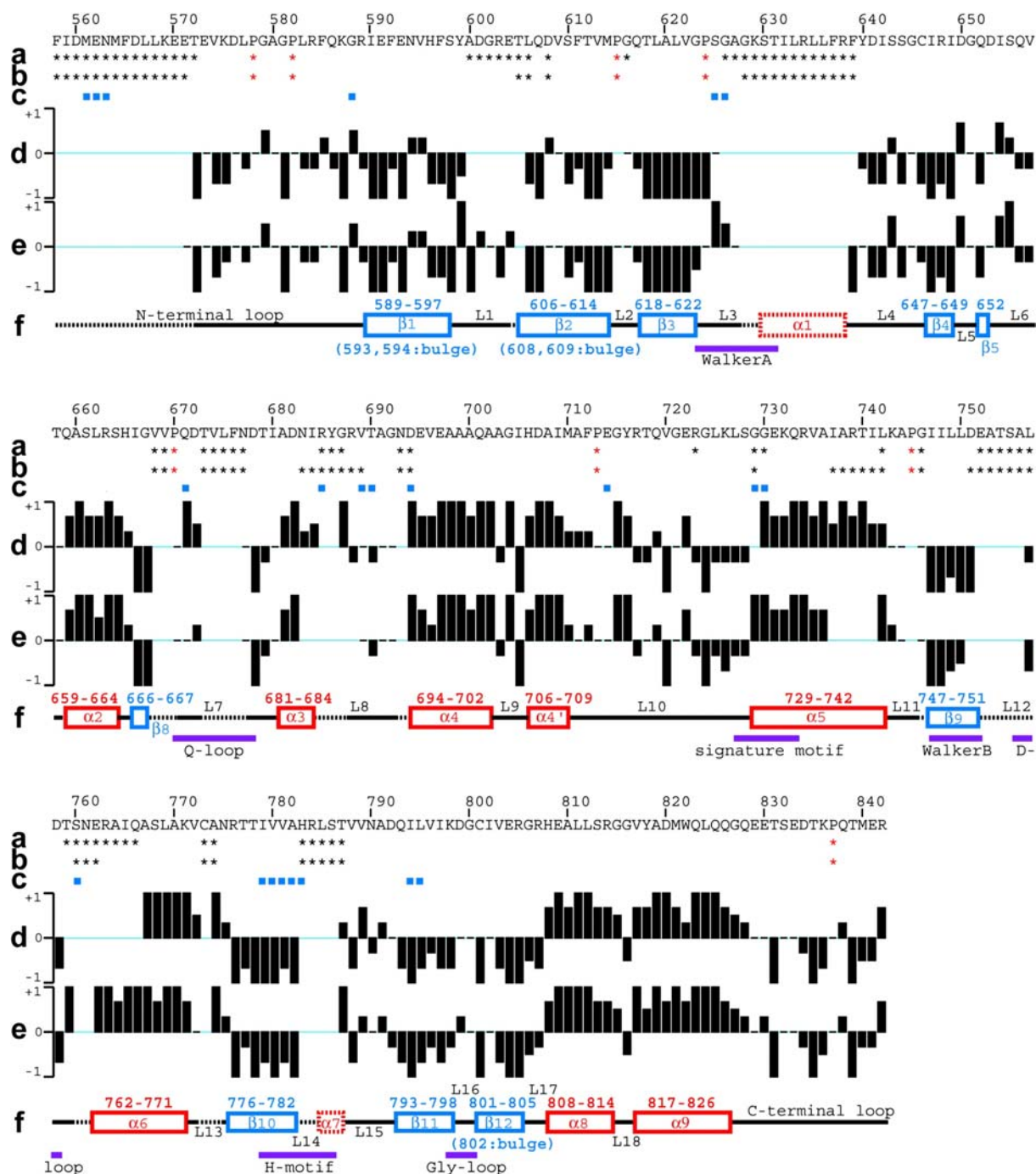


Figure 3. A schematic representation of backbone sequence specific assignment and CSI analysis of ABCB6-C in the nucleotide-free and the ADP-bound states, together with the derived secondary structure elements. (a, b) The residues where no backbone resonances were assigned in the nucleotide-free (a) and the ADP-bound (b) states are represented by asterisks, respectively. Positions of proline residues are also indicated by red asterisks. (c) The residues corresponding to those unassigned in the nucleotide-free state of *Methanococcus jannaschii* MJ1267. (d, f) The consensus CSI (CSI_{ave}) for ABCB6-C in the nucleotide-free (d) and the ADP-bound (e) states, respectively. The CSI_{ave} was calculated according to the following equation, $\text{CSI}_{\text{ave}} = (\text{CSI}^{13\text{C}^{\alpha}} + \text{CSI}^{13\text{C}'} - \text{CSI}^{13\text{C}^{\beta}})/3$. (f) Summary of secondary structure inferred from the CSI data; the red and blue boxes represent the location of α -helices and β -strands, respectively. Each secondary structure element is numbered according to the human TAP1 NBD terminology, and labelled with corresponding residue numbers in ABCB6. Helix $\alpha 1$ and helix $\alpha 7$, which were not identified because of the lack of backbone resonance assignments, are indicated dotted boxes. Loop regions with unassigned residues are also presented with dotted lines. Conserved sequence motifs are shown with purple bars with annotations.

observable $^{13}\text{C}^{\alpha}$, $^{13}\text{C}^{\beta}$ and/or $^{13}\text{C}'$ correlations in the triple resonance spectra, but were difficult to assign because of the multiple assignment possibilities in the amino acid sequence. The remaining cross peaks had a much broader line shape, thus providing scarcely observable cross peaks in the triple-resonance spectra.

The residues with missing assignments were Ile559–Thr572, Ala600–Leu606, Asp608, Gly616, Gly626–Phe639, Val668, Val669, Thr673–Asn677, Arg685–Gly687, Asn693, Asp694, Arg723, Gly729, Gly730, Leu742, Gly746, Asn752–Leu757, Thr759–Gln766, Cys773, Ala774, and His783–Thr787.

The secondary structure of apo-ABCB6-C was predicted from the Chemical Shift Index (CSI) analysis (Wishart and Sykes, 1994) of assigned $^{13}\text{C}^{\alpha}$, $^{13}\text{C}^{\beta}$ and $^{13}\text{C}'$ resonances (Figure 3). Eight helical regions, helix $\alpha 2$ (659–664), $\alpha 3$ (681–684), $\alpha 4$ (694–702), $\alpha 4'$ (706–709), $\alpha 5$ (730–742), $\alpha 6$ (767–771), $\alpha 8$ (808–814) and the C-terminal helix $\alpha 9$ (817–826), were identified, and the relative position of each helix in the amino acid sequence showed good agreement with the position of the corresponding helices in TAP1 NBD (hereinafter, numbering of all secondary elements are adapted to the crystal structures of human TAP1 NBD (Gaudet and Wiley, 2001)). Eleven β -strands, $\beta 1$ (589–592), $\beta 1'$ (595–597), $\beta 2$ (606–614), $\beta 3$ (618–



622), β4 (647–649), β5 (652), β8 (666–667), β9 (747–751), β10 (776–782), β11 (793–798) and β12 (801–805), were also identified, and, again, the relative position of each strand showed good agreement with that of corresponding β-strands in TAP1 NBD.

Three helical regions corresponding to the helix α1, the N-terminal half of the helix α6 and helix α7 of TAP1 NBD (Gaudet and Wiley, 2001) were not identified in ABCB6-C, since the lack of backbone resonance assignments around these three regions prevented the CSI calculations.

Backbone assignment and secondary structure of ABCB6-C in the ADP-bound state

A similar triple-resonance approach was employed for the backbone resonance assignment of ABCB6-C at pH 8.5 and a probe temperature of 25 °C in the presence of excess amount of ADP. Seventy five percent (207 out of 276 non-proline residues) of backbone ^1H , ^{13}C and ^{15}N resonances of ADP-bound ABCB6-C could be assigned. The chemical shift assignments have been deposited in the BioMagResBank database under the accession number BMRB-10017. The ^1H - ^{15}N TROSY-HSQC spectrum of $^2\text{H}/^{13}\text{C}/^{15}\text{N}$ -labelled ADP-bound ABCB6-C is provided as supplementary material with the assignments indicated for the individual cross peaks. Similar to the case in the nucleotide-free state, less than 30 separately observed $^1\text{H}^{\text{N}}$ - ^{15}N correlation cross peaks remained unassigned. Approximately 2/3 of them appeared similar positions of unassigned cross peaks in the nucleotide-free state. Eight cross peaks were unassigned because of the multiple assignment possibilities. The remaining cross peaks were much broader.

The residues with missing assignments were Ile559–Glu571, Thr605, Leu606, Asp608, Gly628–Phe639, Val668, Val669, Val673–Asn677, Asn683–Val689, Asn693, Asp694, Gly729, Ile737–Leu742, Gly746, Asp751–Leu757, Ser760–Glu762, Cys773, Ala774, and His783–Thr787.

The secondary structure of ADP-bound ABCB6-C predicted from the CSI analysis was found to be essentially identical to that of apo-ABCB6-C. As a result, four helical regions, the helix $\alpha 1$, the C-terminal half of the helix $\alpha 3$, five residues in the middle of the helix $\alpha 5$ and $\alpha 7$, were not completely identified because of the lack of backbone resonance assignments.

The missing backbone resonances of ABCB6-C

A surprisingly large number of backbone resonances were missing for both nucleotide-free and ADP-bound states. The incompleteness in the assignments was presumably caused by line broadening of cross peaks in the ^1H - ^{15}N TROSY-HSQC spectra. Wang et al. (2002, 2004) reported a similar incompleteness in the assignments for MJ1267 protein, but for a much smaller number of residues (Figure 3c). Line broadening of NMR resonances is a common phenomenon at regions

involved in conformational multiplicity, when the exchange between the conformations is on an intermediate time scale.

Incomplete exchange of amide ^2H to ^1H during the sample preparation can be ruled out, since the residues with missing assignments are located mainly around the loop regions or the edges of β -sheets, and it is highly unlikely that the amide groups of these residues were involved in tight hydrogen-bond network.

An equally valid explanation of this incompleteness in the assignments is rapid intrinsic backbone amide exchange with water caused by the mildly alkaline (pH 8.5) buffer conditions. Since protection factors are generally lower in loop regions, this possibility must be carefully investigated. The pH dependency of $^1\text{H}^{\text{N}}$ - ^{15}N correlation cross peaks were therefore examined by reducing the sample buffer pH to 8.0 and then 7.5. For the $^1\text{H}^{\text{N}}$ - ^{15}N correlation cross peaks with significant amide-water exchange broadening, the intensity becomes stronger at lower pH conditions. The intensity (the peak height) of the resolved and assigned $^1\text{H}^{\text{N}}$ - ^{15}N correlation cross peaks at pH 7.5 and 8.5 conditions is shown for apo-ABCB6-C (Figure 4a) and ADP-bound ABCB6-C (Figure 4d). In the figure, the intensity at pH 8.5 was normalised relative to that at pH 7.5. In the nucleotide-free state, C-terminal 10–15 residues showed a drastic drop of the intensity at pH 8.5, thereby suggesting that amide-water exchange is significant at this region. In contrast, for the rest of the residues in the nucleotide-free state and almost all of the residues in the ADP-bound state, including the residues surrounding the “unassigned” residues, the intensity was reduced almost equally and the degree of intensity decrease was not so large.

Next, we examined the temperature dependency of $^1\text{H}^{\text{N}}$ - ^{15}N correlation cross peaks, by reducing the probe temperature from 25 to 15 and then 5 °C. In order to follow the chemical shift change during the temperature shift, the backbone resonance assignment was also performed at 5 °C for both apo- and ADP-bound ABCB6-C dissolved in pH 7.5 buffer. The chemical shift assignments in this condition have been also deposited in the BioMagResBank database under the accession number 10016 and 10017, respectively. Note that only a few additional cross peaks were observed under these conditions.

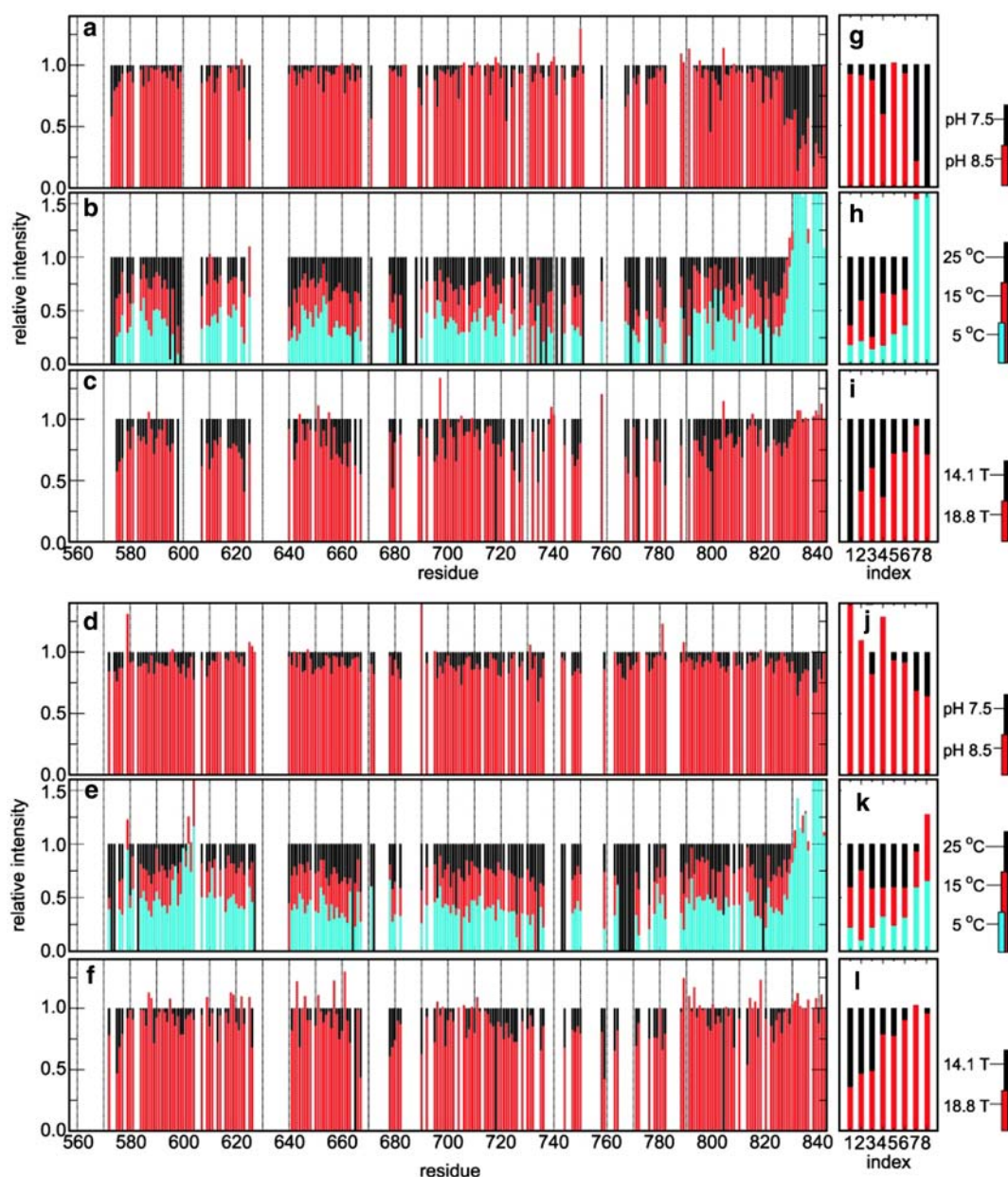


Figure 4. Plots of the pH, temperature and magnetic field strength dependencies of the $^1\text{H}^{\text{N}}\text{-}^{15}\text{N}$ correlation cross peak intensity for observable cross peaks. Data for overlapped cross peaks were excluded from these plots. For the assigned cross peaks of apo-ABCB6-C, (a) pH, (b) temperature, and (c) magnetic field strength dependencies are shown. For the assigned cross peaks of ADP-bound ABCB6-C, data are shown similarly ((d) pH, (e) temperature, and (f) magnetic field strength dependencies). In addition, data are also presented for eight representative unassigned cross peaks for apo-ABCB6-C ((g) pH, (h) temperature, and (i) magnetic field strength) and ADP-bound ABCB6-C ((j) pH, (k) temperature, and (l) magnetic field strength). For pH dependency, the intensity of each cross peak was normalised relative to the intensity at pH 7.5. For temperature dependency, the intensity of each cross peak was normalised relative to the intensity at 25°C. For magnetic field strength dependency, the intensity of each cross peak was normalised assuming that the cross peaks of the C-terminal Arg842 measured at 14.1 T and 18.8 T show identical intensity.

The intensity of NMR signals is generally reduced at lower temperature according to an increase of rotational correlation time. For the cross

peaks with significant amide-water exchange broadening, this decrease in intensity is partly repressed because of the slower exchange rate at

lower temperature. For the cross peaks which are mainly broadened by chemical exchange between multiple conformations, the intensity becomes much weaker, since we are observing “averaged” cross peaks and the slower exchange rate makes the line shape broader. The intensity of $^1\text{H}^{\text{N}}\text{-}^{15}\text{N}$ correlation cross peaks at three different temperatures (5, 15 and 25 °C) is shown for apo-ABCBB6-C (Figure 4b) and ADP-bound ABCB6-C (Figure 4e). The intensity was normalised relative to that at 25 °C. In the nucleotide-free state, the intensity of cross peaks due to the C-terminal 10–20 residues were significantly increased at the lower temperature, which agrees well with the result of the pH-dependency experiments. A similar but moderate change in intensity was observed for the ADP-bound state. For the majority of the rest, both in the nucleotide-free and ADP-bound states, the cross peak intensity was decreased almost uniformly. It is noteworthy that a number of residues showed a remarkable decrease in intensity of cross peaks at lower temperature, and most of them were close to the “missing” regions in the primary structure. For example, residues in the adenine-binding loop (595–599), the Walker A (623, 625, 640 and 641), the helix $\alpha 6$ (763–766), the signature motif (731–735), and the H-motif (780–782, and 789–791) in the nucleotide-free state, and residues in the Walker A (627 and 640), the signature motif (731–735), and the helix $\alpha 5$ (737–742) in the ADP-bound state showed significant decrease in intensity at lower temperature. This result strongly supports the idea of “intermediate” chemical exchange between multiple conformations.

Furthermore, we measured the $^1\text{H}\text{-}^{15}\text{N}$ TROSY-HSQC spectra at 5 °C at a higher magnetic field, 18.8 T (the ^1H frequency of 800 MHz), for comparison with those at 14.1 T (600 MHz). Since magnetic field strength and frequency differences are proportional, the stronger the magnetic field strength becomes, the more the line shape broadens for the cross peaks with chemical exchange. For the two magnetic fields, 14.1 and 18.8 T, the intensities of all resolved and sequentially assigned cross peaks were obtained and normalised relative to that of the C-terminal residue, Lys842, as shown in Figure 4c (apo-ABCB6-C) and Figure 4f (ADP-bound ABCB6-C). Again, a number of residues surrounding the “missing” loops exhibited weaker cross peaks at 18.8 T than at 14.1 T. Particularly, residues around the Q-loop (residues

665, 667 and 679 in apo-ABCB6-C and residues 667, 678 and 679 in ADP-ABCB6-C) showed a significant decrease in intensity at 18.8 T.

For the observed but unassigned $^1\text{H}^{\text{N}}\text{-}^{15}\text{N}$ correlation cross peaks, the pH (Figure 4g, j), temperature (Figure 4h, k) and magnetic field strength (Figure 4i, l) dependencies were also examined. For each state, data of eight representative cross peaks are shown. Some cross peaks show broader line shape at higher pH and increased intensity at lower temperature, thereby categorising them into a group showing rapid amide-water exchange. In addition, there were cross peaks showing relatively small pH dependency, weaker intensity at lower temperature and higher magnetic field strength, which are explainable by assuming the existence of chemical exchange between multiple conformations. Figure 5 shows a region of $^1\text{H}\text{-}^{15}\text{N}$ TROSY-HSQC of apo-ABCB6-C, where an unassigned cross peak (the data for this cross peak is indicated as index #2 in Figure 4g–i) is observed, measured at (a) 600 MHz, 25 °C and pH 7.5, (b) 600 MHz, 15 °C and pH 7.5, (c) 600 MHz, 5 °C and pH 7.5, (d) 600 MHz, 25 °C and pH 8.5, and (e) 800 MHz, 5 °C and pH 7.5. The pH, temperature and magnetic field dependencies of this unassigned cross peak show typical behaviour when assuming an “intermediate” chemical exchange.

From these temperature and magnetic field dependencies of the $^1\text{H}^{\text{N}}\text{-}^{15}\text{N}$ correlation cross peaks, we concluded that the cross peaks of the “unassigned” residues were extremely broadened mainly because of a chemical exchange at an “intermediate” rate on the NMR time scale, and were therefore unobservable. As the conversion rate is remarkably slow, the exchange is probably between two or more stable conformations of the regions.

Discussion

Local conformational multiplicity found for the nucleotide-free ABCB6-C

The residues with missing backbone assignments in the nucleotide-free state were mapped onto the homology modelled structure of ABCB6-C (Figure 6a). It was particularly interesting that the majority of these “missing cross peaks” were

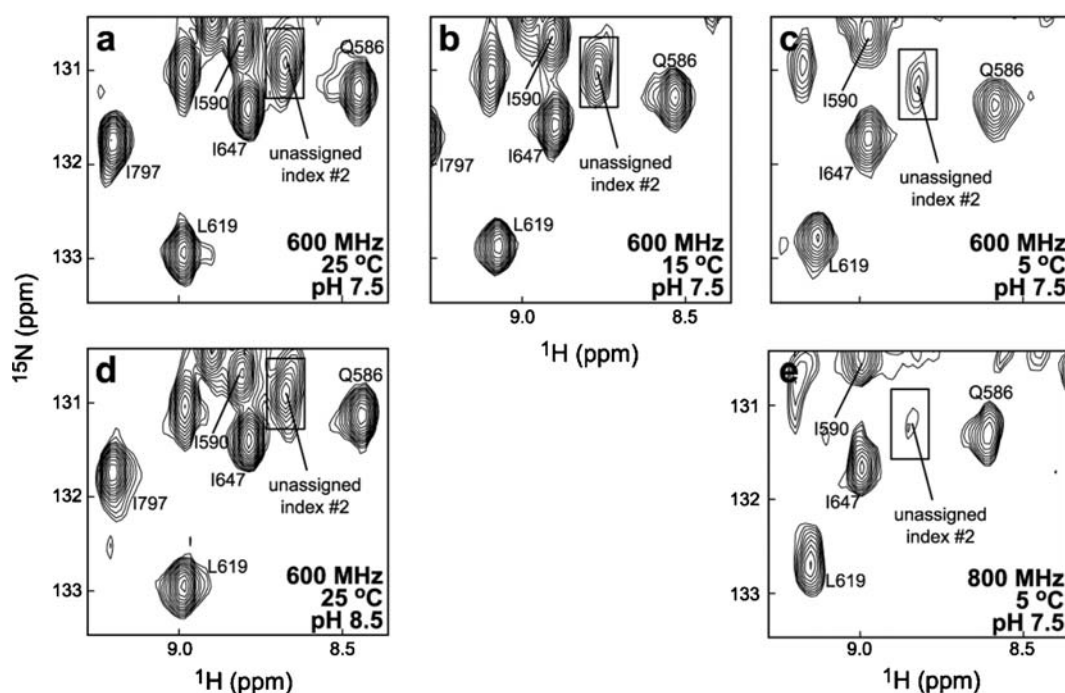


Figure 5. Contour plots of a region of ^1H - ^{15}N TROSY-HSQC spectra of apo-ABCB6-C measured (a) 600 MHz, 25 °C and pH 7.5, (b) 600 MHz, 15 °C and pH 7.5, (c) 600 MHz, 5 °C and pH 7.5, (d) 600 MHz, 25 °C and pH 8.5, and (e) 800 MHz, 5 °C and pH 7.5. The assignment of each cross peak is shown in each spectrum with the exception of an unassigned cross peak, which is indicated by a box.

located over a wide area on one side of the protein surface; around the N-terminal loop, loop L1, loop L3-helix α 1, strand β 8-loop L7, loop L8, helix α 5, loop L12, loop L13, and loop L14-helix α 7.

Extreme line broadening of the N-terminal 14 residues is presumably due to the conformational flexibility of this region caused by the N-terminal truncation. Considering the rest of the “missing” residues, it is obvious that the majority of them are responsible for nucleotide-binding. Indeed, residues 600–606 (in loop L1) follow the Tyr599 residue that is conserved among the NBDs and strongly suggested to be responsible for adenine base binding (this loop L1 is henceforth referred to as adenine-binding loop). Residues 626–639 (in loop L3 and helix α 1) include the Walker A motif, which is proposed to bind to α - and β -phosphates. Residues 668–669 and 673–677 are involved in the Q-loop (loop L7), which is responsible for γ -phosphate binding and presumably for ATP hydrolysis. Residues 729–730 are in the middle of the signature motif. Residues 752–(758)–766 locate around loop L12 (sometimes referred to as the D-loop) following the Walker B motif. Residues 783–787 (in loop L14 and helix α 7) are involved in

the switch region or the H-motif (His783 is suggested to be the conserved histidine residue). Arg723 in loop L10 is the highly conserved arginine residue. The role of this residue has been discussed in the X-ray studies, and conformational cooperativity between this arginine and the Q-loop has been proposed (Karpowich et al., 2001). In addition, residues 773–774 are actually in the vicinity of the N-terminal end of the Q-loop.

The “missing-backbone-resonance” phenomenon in the nucleotide-binding pocket can be understood by hypothesising a conformational multiplicity and chemical exchange line-broadening around this region. Indeed, Wang et al. reported that the backbone resonances for a total of 23 non-proline residues, the majority of which are located around the region responsible for the interaction of the adenine moiety, the Walker A motif, the Q-loop, the signature motif, the D-loop and the H-motif, were not assigned for MJ1267 in the nucleotide-free state (Figure 3c) (Wang et al., 2002). In addition, from the ^{15}N -relaxation analysis, they found that residues with significantly large exchange contributions were mostly located around the above mentioned key functional

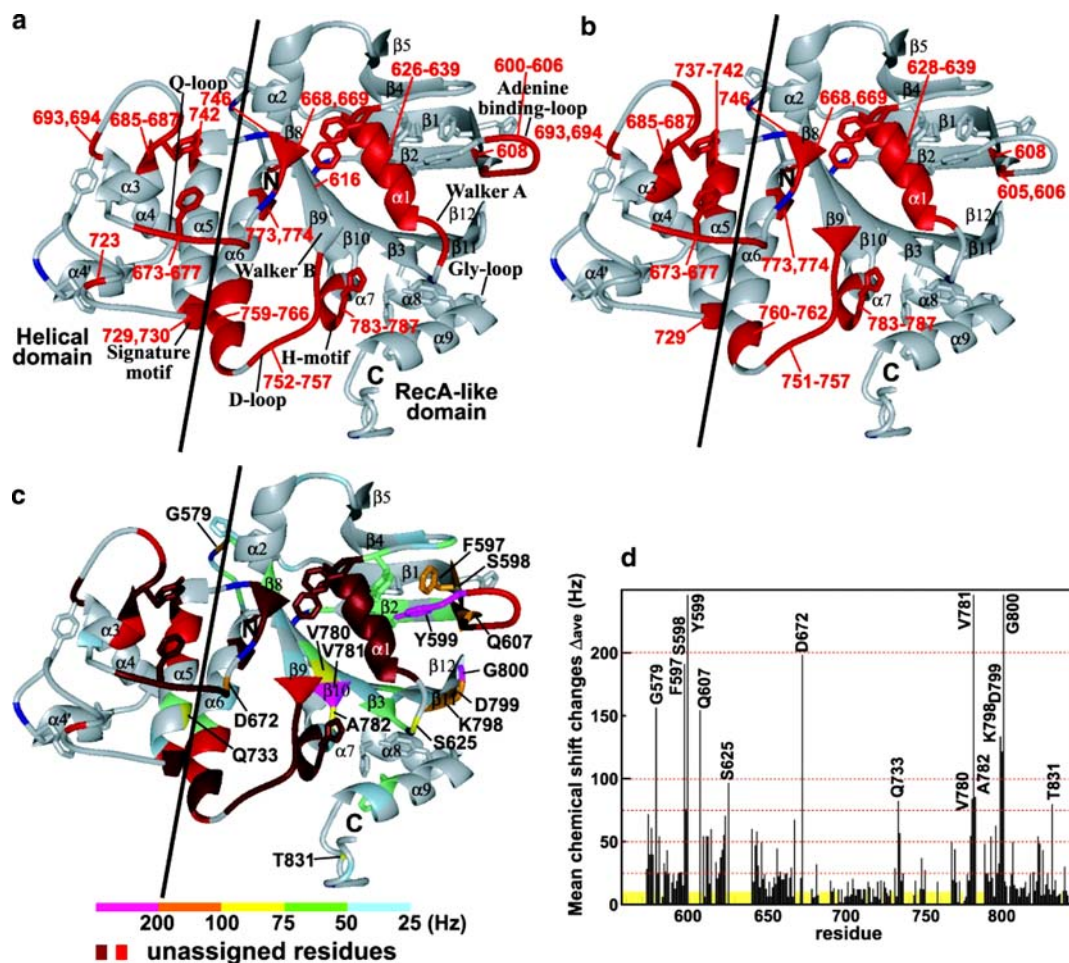


Figure 6. Distributions of residues for which backbone resonances were not assigned in the nucleotide-free (a) and the ADP-bound (b) states are coloured by red on a ribbon model of the homology modelled structure of ABCB6-C. Aromatic side-chains are also shown. Proline residues are colour-coded in dark blue. Positions of conserved motifs as well as the border separating the RecA-like domain and the Helical domain are indicated. Chemical shift perturbation for backbone $^1\text{H}^{\text{N}}$ and ^{15}N nuclei of ABCB6-C upon ADP binding. (c) ABCB6-C residues affected upon ADP binding mapped onto the homology modelled ABCB6-C structure. The mean shift difference, Δ_{ave} , for each amino acid residue was calculated as $[(\Delta^1\text{H}^{\text{N}})^2 + (\Delta^{15}\text{N})^2]^{1/2}$, where $\Delta^1\text{H}^{\text{N}}$ and $\Delta^{15}\text{N}$ are the chemical shift differences (Hz) between the nucleotide-free ABCB6-C and the ABCB6-C + ADP mixture at protein:nucleotide molar ratios of 1:32 for $^1\text{H}^{\text{N}}$ and ^{15}N resonances observed at 14.1T (^1H frequency is 600 MHz), respectively. The colour coding is as follows: white ($\Delta_{ave} < 25$ Hz); light blue ($25 \text{ Hz} \leq \Delta_{ave} < 50$ Hz); green ($50 \text{ Hz} \leq \Delta_{ave} < 75$ Hz); yellow ($75 \text{ Hz} \leq \Delta_{ave} < 100$ Hz); orange ($100 \text{ Hz} \leq \Delta_{ave} < 200$ Hz); magenta ($\Delta_{ave} \geq 200$). Largely perturbed residues ($\Delta_{ave} \geq 75$) were labelled with residue numbers. The residues for which backbone resonances were not assigned in both the nucleotide-free and the ADP-bound states are shown in dark red, while those unassigned in the either state are shown in red. Aromatic side-chains are also shown. Proline residues are colour-coded in dark blue. (d) Bar graph of Δ_{ave} values against amino acid residues. Bars representing largely perturbed residues ($\Delta_{ave} \geq 75$) were labelled with residue numbers. The residues for which backbone resonances were not assigned in both the nucleotide-free and the ADP-bound states are indicated in yellow. Molecular graphics images were produced using the MidasPlus software from the Computer Graphics Laboratory, University of California, San Francisco.

motifs, which directly suggests a chemical exchange between multiple conformations (Wang et al., 2004). The conformational flexibility of these regions is also supported by the fact that relatively high thermal B -factors are observed for these regions in the crystal structures of NBDs in

the nucleotide free state (Karpowich et al., 2001; Schmitt et al., 2003). In the case of ABCB6-C, it is noteworthy that the backbone resonances were not assigned for the whole region of the helix $\alpha 1$, which follows the Walker A motif. It is unlikely that the backbone structure of this helix is highly

flexible, since small thermal *B*-factors are commonly found for this helix region of the NBD crystal structures. A possible answer for this phenomenon might be the flexibility in side-chain orientation of aromatic residues clustered around this helix (Phe597, Tyr599, Phe637, Phe639 and Tyr640), which consequently alters the ring current effects from the aromatic rings and thereby provides large chemical shift changes.

Apart from the residues mentioned above, residues, 685–687 (in loop L8), 693–694 (in loop L8) and 742 (in loop L12) are close to each other and located on the Helical domain (or ABC α -subdomain), thereby distant from the ATPase core domain (or RecA-like domain), which includes the conserved motifs responsible for nucleotide-binding. Again, Wang et al., reported that the backbone resonances for residues Leu104, Ile108, Asn109, Ser117 and Leu118, which located at a similar position in the Helical domain, were not assigned for MJ1267 protein (Figure 3c) (Wang et al., 2002). The “missing” residues in the Helical domain are discussed in conjunction with the results from the ADP-bound state in the following paragraphs.

Local conformational multiplicity found for ADP-bound ABCB6-C

In a similar manner to that employed for the nucleotide-free ABCB6-C, the residues with missing backbone assignments in the ADP-bound state were mapped onto the homology modelled structure of ABCB6-C (Figure 6b).

There are four significant changes in the distribution of “missing” residues between the nucleotide-free and the ADP-bound states. First, the backbone resonances were easily assigned for residues 600–604 (L1/adenine-binding loop). Second, two residues involved in the Walker A motif, Gly626 and Ala627, are now “observable”. Third, Gly730 in the signature motif and neighbouring residues, Arg763–Gln766, showed assignable backbone resonances. And in contrast, the “missing” region was expanded to residues, Asn683, Ile684, Arg688 and Val689, in loop L8 and also residues, Ile737–Ile741, in helix α 5 in the Helical domain.

The first and second changes can be explained by the conformational stabilisation of the adenine-binding loop and the Walker A motif upon

ADP-binding. For MJ1267 protein, Wang et al. reported a similar appearance of backbone resonances for residue Gly43 (corresponding to residue Gly626 in ABCB6-C) in the ADP-bound state, while they were not observable in the nucleotide-free state (Wang et al., 2004). They also described that the exchange contributions for the residues in the adenine-binding loop and the D-loop became insignificant. Similar events have been observed and discussed in some X-ray crystallographic studies on MJ1267 (Karpowich et al., 2001). The backbone thermal *B*-factors in the adenine-binding loop (residues 17–20), the Walker A and B motifs and the H-motif are among the lowest in the ADP bound state but are all substantially elevated in the nucleotide-free structure, where each of these segments corresponds to a new local maximum in the *B*-factor plot. They concluded that the region surrounding the ATPase active site in MJ1267 is substantially more flexible in the absence of bound nucleotide in addition to having a different equilibrium conformation.

The third change is more complex. Residues Gly730 (in the signature motif) and Arg763–Gln766 (in helix α 6) are located around the interface of the ATPase core domain and the Helical domain, where rigid body rotation correlating to the nucleotide-binding event has been proposed (Yuan et al., 2001; Gaudet and Wiley, 2001; Karpowich et al., 2001). Relatively high thermal *B*-factors are commonly found around the region in various crystal structures, suggesting that this region is potentially flexible (Gaudet and Wiley, 2001; Karpowich et al., 2001). Our NMR observations that backbone resonances of this region were hardly observable in the nucleotide-free state but were assignable in the ADP-bound state suggests at least two possibilities. First, a kind of structural stabilisation may occur around this region as a result of ADP-binding. Second, altered orientation of the Q-loop, which is in the vicinity of residues Gly730 and Arg763–Gln766, between the nucleotide-free and the ADP-bound states may affect the exchange regime of backbone resonances of these residues. X-ray studies have proposed that the Q-loop may function as a γ -phosphate linker, and alter its conformation largely corresponding to its nucleotide-binding state, which suggests that the second possibility we propose is more credible (Karpowich et al., 2001; Smith et al., 2002).

Crystal structures have shown that maximum thermal B -factors are commonly found in the region connecting helices $\alpha 3$ and $\alpha 4$, suggesting that this region is the most “flexible” part in NBD structures (Gaudet and Wiley et al., 2001; Karpowich et al., 2001). In particular, MJ1267 protein, which has the LivG insert in the region, showed significant chemical shift broadenings for the region both for the nucleotide-free and the ADP-bound states in aqueous solution (Wang et al., 2004). Coincidentally, our NMR observation showed that residues Arg685–Gly687, Asn693–Asp694 (in loop L8), and Leu642 (in helix $\alpha 5$) give no detectable backbone resonances both in the nucleotide-free and ADP-bound states, presumably caused by local conformational changes on an intermediate NMR time scale.

Finally, it is worth noting the difference in appearance of the backbone resonances of the C-terminal ~ 15 residues; significantly broadened in the nucleotide-free state, while distinctly visible in the ADP-bound state. This suggests a kind of interaction between the C-terminal residues with the other part of protein surface in the nucleotide-free state, but with no or very weak interactions in the ADP-bound state. From the modelled structure, these C-terminal residues can be close to either the Walker A, H-motif or D-loop. An interaction of the C-terminal region with these nucleotide-binding motifs can be therefore assumed in the absence of adenine nucleotide.

Chemical shift perturbation upon ADP-binding

For all the backbone assigned residues both in the nucleotide-free and the ADP bound states, the mean differences in $^1\text{H}^{\text{N}}$ and ^{15}N chemical shifts, Δ_{ave} , was calculated and mapped onto the homology-modelled ABCB6-C structure, together with the information from “missing” residues (Figure 6c, d). For the sake of ensuing discussions, the residues are arbitrarily classified on the basis of their degree of chemical shift perturbation into unperturbed ($\Delta_{\text{ave}} < 25$ Hz), least perturbed ($25 \text{ Hz} \leq \Delta_{\text{ave}} < 50$ Hz), moderately perturbed ($50 \text{ Hz} \leq \Delta_{\text{ave}} < 75$ Hz), largely perturbed ($75 \text{ Hz} \leq \Delta_{\text{ave}} < 100$ Hz) and severely perturbed ($\Delta_{\text{ave}} \geq 100$ Hz) and colour-coded as described in Figure 6 (^1H and ^{15}N frequencies were 600.13 MHz and 60.80645 MHz, respectively). There were three residues, Tyr599 (in loop L1),

Val781 (in strand $\beta 7$), and Gly800 (in loop L16), which showed the $\Delta_{\text{ave}} > 200$ Hz.

As expected, some of the severely perturbed residues were from regions neighbouring the “missing” residues. Starting from the residues contributing to the adenine-ring binding, Phe597, Ser598, Tyr599 in loop L1 and Gln607 in strand $\beta 1$, which locates near the adenine binding loop, are significantly perturbed by ADP binding. Tyr599 is indeed the residue proposed to be responsible for direct adenine-base binding. Ser625, located in the Walker A motif, also showed significant perturbation. Lys798, Asp799 and Gly800 in loop L16 were also perturbed. Loop L16 (Lys798–Gly800 in ABCB6-C) is otherwise described as Gly-loop, and in the case of HlyB, an interaction was identified between a glycine residue (Gly679) in the Gly-loop and a serine residue (Ser506) in the Walker A motif (Schmitt et al., 2003). These glycine and serine residues are also conserved in ABCB6, therefore suggesting a similar interaction in ABCB6-C. Though Gln671 in the Q-loop showed least perturbation, the next residue, Asp672, as well as the structurally neighbouring residue, Gln733 in helix $\alpha 5$, showed large perturbation, presumably reflecting the conformational re-orientation of the Q-loop induced upon ADP-binding.

Val780, Val781 and Ala782 locate prior to the “missing” H-motif, which has been postulated to polarise the attacking water molecule for hydrolysis (Hopfner et al., 2000; Smith et al., 2002). Since it has been suggested that these two motifs, the Q-loop and the H-motif, are involved in the binding and hydrolysis of γ -phosphate, it is difficult to explain why large chemical shift changes were found for these regions upon ADP-binding. However, Wang et al. showed relatively large chemical shift perturbations for the Q-loop and the H-motif for MJ1267 upon ADP-binding (Wang et al., 2004), and some X-ray studies on the ADP-bound states of NBDs have also described the conformational changes of these regions upon ADP-binding (Gaudet and Wiley et al., 2001; Karpowich et al., 2001). In addition, the large chemical shift perturbation for Gly579 and Thr831 may be reflected by the flexible conformation of N- and C-terminal residues. The large perturbation of residues in the above mentioned regions, suggests that extensive local conformational changes upon ADP binding may be involved around the nucleotide binding region.

The residues displaying moderate perturbations ($50 \text{ Hz} \leq \Delta_{\text{ave}} < 75 \text{ Hz}$) are mainly located in the ATPase core domain but not the Helical domain, and neighbouring the regions for which backbone resonances were unobservable (Walker A, Q-loop, Walker B, H-motif, and adenosine-binding region). In our NMR observations, most of the severely and largely perturbed residues are localised to areas surrounding the regions lacking backbone resonance assignments. This reinforces the idea that these functional loops and motifs are directly involved in ADP-binding, and consequently local conformation of these regions are also perturbed, even though corresponding backbone resonances were not observable because of the chemical exchange regime.

Conclusion

We have overexpressed and purified the 31.5 kDa protein fragment of ABCB6 comprising residues Phe558 to Arg842, including the nucleotide binding domain. Backbone ^1H , ^{13}C and ^{15}N resonance assignments have been performed for both nucleotide-free and ADP-bound forms of this relatively large protein fragment, providing an excellent probe for the investigation of conformational changes upon nucleotide-binding. The prediction of secondary structure by the CSI method showed good agreement with other NBDs. A homology modelling approach was employed to produce a reasonable three dimensional model structure of ABCB6-C, which was utilised for the interpretation of the exchange broadening of backbone resonances and the chemical shift perturbation upon ADP-binding.

In the nucleotide-free state, backbone resonances were not observed for approximately 25% of non-proline residues, almost all of which were located in loop structures and classified broadly into two categories; residues contributing to the nucleotide-binding and γ -phosphate hydrolysis or residues located in the Helical domain. The pH, temperature and magnetic field dependencies of $^1\text{H}^{\text{N}}\text{-}^{15}\text{N}$ correlation cross peaks strongly suggest localised conformational multiplicity and exchange on an intermediate time scale around the loop regions. Upon ADP-binding, the regions responsible for adenine ring- and α/β -phosphate binding were partially stabilised, while the

backbone resonances for the rest of the nucleotide-binding loop regions and the residues in the Helical domain were still “unassigned”. These results indicate that the localised conformational multiplicity still remains in the ADP-bound state. Relatively large chemical shift changes of $^1\text{H}^{\text{N}}\text{-}^{15}\text{N}$ correlation cross peaks were observed for the residues which are located adjacent to the “unassigned” residues, while the CSI analysis showed that the secondary structure elements remain essentially identical in the transition from the nucleotide-free to the ADP-bound states. These results suggest that ADP-binding induced substantial conformational changes around nucleotide-binding loop regions and, possibly, around the “unassigned” residues in the Helical domain.

In comparison with the ^{15}N -relaxation study of MJ1267 (Wang et al., 2004), we conclude that the dynamic property providing the significant exchange broadening to the backbone resonances of the residues in the key ABC motifs in MJ1267 is essentially the same as that induced our “missing-backbone-resonance” phenomenon in ABCB6-C. Since MJ1267 is from the hyperthermophilic organism *Methanococcus jannaschii*, and stable during the NMR measurement at higher probe temperature (40 °C), backbone resonances were relatively more “averaged” and presumably observable with enough intensity for the ^{15}N -relaxation experiments, which cannot be confirmed because of the very short lifetime of ABCB6-C at higher temperature. As was emphasised in the ^{15}N -relaxation study of MJ1267, the most remarkable thing is that this dynamic property is observed for both adenine nucleotide-binding loops and the Helical domain, which are distant in space from each other. This “cooperativity” is presumably mediated by the Q-loop. In the nucleotide-free state, the Helical domain and the adenine nucleotide-binding loops (including the Q-loop, which connects the RecA-like domain and the Helical domain) have a conformational multiplicity. In the ADP-bound state, “induced-fit” fixation of conformations occurs in the regions responsible for binding to adenine-ring and α/β -phosphate groups. When ATP binds to the nucleotide-free state, “induced-fit” fixation also occurs in the H-motif, D-loop and Q-loop by the interaction with γ -phosphate via water molecules, and the consequent rearrangement of the conformation of the Q-loop alters the relative orientation of the

Helical domain changing its interaction with the TMD. This cooperativity may explain the mechanism whereby information regarding binding states is transmitted between the NBD and the TMD, e.g. the ATP-binding at the NBD and the substrate-binding at the TMD, the ATP hydrolysis at the NBD and the structural rearrangement of the TMD. Further, the ATP-induced rearrangement of the Q-loop as well as the changes in the Helical domain may perturb the conformation of the neighbouring signature motif, which can be a “trigger” to promote the closed dimer formation.

In summary, we revealed that this dynamic cooperativity, which has been discovered for a prokaryotic ATP-binding cassette, MJ1267, also exists in the NBD of a higher eukaryotic ABC transporter, and presumably shared by all members of ABC transporters.

Acknowledgements

The authors express their sincere gratitude to Dr N. Mitsuhashi for the DNA encoding ABCB6-C. We thank Dr Brian Smith for valuable support on the analysis using ANSIG software, Dr Daniel Nietlispach for setting up triple-resonance NMR experiments with TROSY scheme, Prof. Masatsune Kainosho for the measurements on the DRX800 spectrometer in the CREST NMR facility at Tokyo Metropolitan University, and Takeshi Nishimura for the modification of original ANSIG to run in an OpenGL/X WINDOW system environment. We are grateful to Drs Brian Smith and Jonathan Heddle, for a critical reading of this manuscript. This work was supported in part by Grants-in-Aid for Scientific Research in Priority Areas “Molecular Interactions Regulating Membrane Interface of Biological Systems” from the Ministry of Education, Culture and Sports, Science and Technology, and grants from the Molecular Ensemble Program, RIKEN and CREST, Japan Science and Technology (JST) to Y.I.

References

Allikmets, R., Raskind, W.H., Hutchinson, A., Schueck, N.D., Dean, M. and Koeller, D.M. (1999) *Hum. Mol. Gen.* **8**, 743–749.

Altschul, S.F., Madden, T.L., Schaffer, A.A., Zhang, J., Zhang, Z., Miller, W. and Lipman, D.J. (1997) *Nucleic Acids Res.* **25**, 3389–3402.

Barna, J.C., Laue, E.D., Mayger, M.R., Skilling, J. and Worrall, S.J.P. (1987) *J. Magn. Reson.* **73**, 69–77.

Bax, A. and Ikura, M. (1991) *J. Biomol. NMR* **1**, 99–104.

Beinert, H. and Kiley, P.J. (1999) *Curr. Opin. Chem. Biol.* **3**, 152–157.

Beinert, H., Holm, R.H. and Munck, E. (1997) *Science* **277**, 653–659.

Canutescu, A.A., Shelenkov, A.A. and Dunbrack, R.L. Jr. (2003) *Protein Sci.* **12**, 2001–2014.

Chang, G. (2003) *J. Mol. Biol.* **330**, 419–430.

Chang, G. and Roth, C.B. (2001) *Science* **293**, 1793–1800.

Chen, C.-A. and Cowan, J.A. (2003) *J. Biol. Chem.* **278**, 52681–52688.

Clubb, R.T., Thanabal, V. and Wagner, G. (1992) *J. Magn. Reson.* **97**, 213–217.

Csere, P., Lill, R. and Kispal, G. (1998) *FEBS Lett.* **441**, 266–270.

Dean, M., Rzhetsky, A. and Allikmets, R. (2001) *Genome Res.* **7**, 1156–1166.

Gaudet, R. and Wiley, D.C. (2001) *EMBO J.* **20**, 4964–4972.

Geyer, M., Schweins, T., Herrmann, C., Prisner, T., Wittinghofer, A. and Kalbitzer, H.R. (1996) *Biochemistry* **35**, 10308–10320.

Golovanov, A.P., Hautbergue, G.M., Wilson, S.A. and Lian, L.Y. (2004) *J. Am. Chem. Soc.* **126**, 8933–8939.

Grzesiek, S. and Bax, A. (1992) *J. Magn. Reson.* **96**, 432–440.

Grzesiek, S., Anglister, J., Ren, H. and Bax, A. (1993) *J. Am. Chem. Soc.* **115**, 4369–4370.

Higgins, C.F. and Linton, K.J. (2004) *Nat. Struct. Mol. Biol.* **11**, 918–926.

Holland, I.B. and Blight, M.A. (1999) *J. Mol. Biol.* **22**, 381–399.

Hopfner, K.P., Karcher, A., Shin, D.S., Craig, L., Arthur, L.M., Carney, J.P. and Tainer, J.A. (2000) *Cell* **101**, 789–800.

Hung, L.W., Wang, I.X., Nikaido, K., Liu, P.Q., Ames, G.F. and Kim, S.H. (1998) *Nature* **396**, 703–707.

Ikura, M., Kay, L.E. and Bax, A. (1990) *Biochemistry* **29**, 4659–4667.

Ito, Y., Yamasaki, K., Iwahara, J., Terada, T., Kamiya, A., Shirouzu, M., Muto, Y., Kawai, G., Yokoyama, S., Laue, E.D., Wälchli, M., Shibata, T., Nishimura, S. and Miyazawa, T. (1997) *Biochemistry* **36**, 9109–9119.

James, L.C. and Tawfik, D.S. (2003) *Trends Biochem. Sci.* **28**, 361–368.

Karpowich, N., Martsinkevich, O., Millen, L., Yuan, Y.-R., Dai, P.L., MacVey, K., Thomas, P.J. and Hunt, J.F. (2001) *Structure* **9**, 571–586.

Kelly, A., Powis, S.H., Kerr, L.A., Mockridge, I., Elliott, T., Bastin, J., Uchanska-Ziegler, B., Ziegler, A., Townsley, J. and Townsend, A. (1992) *Nature* **355**, 641–644.

Kispal, G., Csere, P., Guiard, B. and Lill, R. (1997) *FEBS Lett.* **418**, 346–350.

Kispal, G., Csere, P., Prohl, C. and Lill, R. (1999) *EMBO J.* **18**, 3981–3989.

Kraulis, P.J. (1989) *J. Magn. Reson.* **24**, 627–633.

Kraulis, P.J., Domaille, P.J., Campbell-Burk, S.L., van Aken, T. and Laue, E.D. (1994) *Biochemistry* **33**, 3515–3531.

Laue, E.D., Mayger, M.R., Skilling, J. and Staunton, J. (1996) *J. Magn. Reson.* **68**, 14–29.

Leighton, J. and Schatz, G. (1995) *EMBO J.* **14**, 188–195.

- Lewis, H.A., Buchanan, S.G., Burley, S.K., Conners, K., Dickey, M., Dorwart, M., Fowler, R., Gao, X., Guggino, W.B., Hendrickson, W.A., Hunt, J.F., Kearins, M.C., Lorimer, D., Maloney, P.C., Post, K.W., Rajashankar, K.R., Rutter, M.E., Sauder, J.M., Shriver, S., Thibodeau, P.H., Thomas, P.J., Zhang, M., Zhao, X. and Emtage, S. (2004) *EMBO J.* **23**, 282–293.
- Madej, T., Gibrat, J.F. and Bryant, S.H. (1995) *Proteins* **23**, 356–369.
- Matsuo, H., Li, H. and Wagner, G. (1996) *J. Magn. Reson. Ser. B* **110**, 112–115.
- Mitsuhashi, N., Miki, T., Senbongi, H., Yokoi, N., Yano, H., Miyazaki, M., Nakajima, N., Iwanaga, T., Yokoyama, Y., Shibata, T. and Seino, S. (2000) *J. Biol. Chem.* **275**, 17536–17540.
- Pervushin, K., Riek, R., Wider, G. and Wüthrich, K. (1997) *Proc. Natl. Acad. Sci. USA* **94**, 12366–12371.
- Rovnyak, D., Frueh, D.P., Sastry, M., Sun, Z.Y., Stern, A.S., Hoch, J.C. and Wagner, G. (2004) *J. Magn. Reson.* **170**, 15–21.
- Šali, A. and Blundell, T.L. (1993) *J. Mol. Biol.* **234**, 779–815.
- Salzmann, M., Wider, G., Pervushin, K. and Wüthrich, K. (1999a) *J. Biomol. NMR* **15**, 181–184.
- Salzmann, M., Wider, G., Pervushin, K., Senn, H. and Wüthrich, K. (1999b) *J. Am. Chem. Soc.* **121**, 844–848.
- Schmieder, P., Stern, A.S., Wagner, G. and Hoch, J.C. (1994) *J. Biomol. NMR* **4**, 483–490.
- Schmitt, L., Benabdelhak, H., Blight, M.A., Holland, I.B. and Stubbs, M.T. (2003) *J. Mol. Biol.* **330**, 333–342.
- Schneider, E. and Hunke, S. (1998) *FEMS Microbiol. Rev.* **22**, 1–20.
- Senbongi, H., Ling, F. and Shibata, T. (1999) *Mol. Gen. Genet.* **262**, 426–436.
- Smith, P.C., Karpowich, N., Millen, L., Moody, J.E., Rosen, J., Thomas, P.J. and Hunt, J.F. (2002) *Mol. Cell.* **10**, 139–149.
- Stohs, S.J. and Bagchi, D. (1995) *Free Radic. Biol. Med.* **18**, 321–336.
- Tomii, K. and Akiyama, Y. (2004) *Bioinformatics* **20**, 594–595.
- van Veen, H.W., Callaghan, R., Soceneantu, L., Sardini, A., Konings, W.N. and Higgins, C.F. (1998) *Nature* **391**, 291–295.
- Wang, C.Y., Hunt, J.F., Rance, M. and Palmer, A.G. (2002) *J. Biomol. NMR* **24**, 167–168.
- Wang, C., Karpowich, N., Hunt, J.F., Rance, M. and Palmer, A.G. (2004) *J. Mol. Biol.* **342**, 525–537.
- Wishart, D.S. and Sykes, B.D. (1994) *J. Biomol. NMR* **4**, 171–180.
- Wittekind, M. and Mueller, L. (1993) *J. Magn. Reson. Ser. B* **101**, 201–205.
- Yamazaki, T., Lee, W., Revington, M., Mattiello, D.L., Dahlquist, F.W., Arrowsmith, C.H. and Kay, L.E. (1994a) *J. Am. Chem. Soc.* **116**, 6464–6465.
- Yamazaki, T., Lee, W., Arrowsmith, C.H., Muhandiram, D.R. and Kay, L.E. (1994b) *J. Am. Chem. Soc.* **116**, 11655–11666.
- Yuan, Y.R., Blecker, S., Martsinkevich, O., Millen, L., Thomas, P.J. and Hunt, J.F. (2001) *J. Biol. Chem.* **276**, 32313–32321.
- Zhu, G. and Bax, A. (1990) *J. Magn. Reson.* **100**, 202–207.